

## Structural changes accompanying densification of random hard-sphere packings

Andrew S. Clarke\* and Hannes Jónsson†

*Department of Chemistry, BG-10, University of Washington, Seattle, Washington 98195*

(Received 30 December 1991)

Local icosahedral order is found to increase as random hard-sphere packings (one- and two-component) generated on the computer are densified from the (recently established) “loose random-packing” limit to the “dense random-packing” limit. While icosahedral ordering in “atomic” systems is frequently ascribed to the energetic stability of icosahedral clusters, the present results show that icosahedral ordering can arise from packing constraints alone. However, the icosahedra are often distorted, partly due to the lack of preferred distance between hard spheres. At high density one-third to one-half of the pairs in the first peak of the radial distribution function (RDF) are icosahedral fragments. The splitting of the second peak, which is characteristic of packings of spherical particles, was studied by decomposing the RDF into components according to the local environment of the pairs. Linear trimers of spheres are responsible for the second subpeak while the first subpeak arises roughly equally from tetrahedra sharing a face and triangles with adjacent sides. The hard-sphere packings were compared with packings of soft, attracting spheres by relaxing the configurations under a Lennard-Jones potential. The fraction of pairs characteristic of local crystalline order in the first peak of the RDF was found to increase. The reversal of the relative height of the two parts of the split second peak results from a broadening of the distribution of distances within the linear trimers, while the distribution sharpens for the face sharing tetrahedra and adjacent triangles.

PACS number(s): 64.60.Cn, 81.20.Ev, 82.70.Kj, 64.70.Pf

### I. INTRODUCTION

Packings of hard spheres have been studied extensively because they serve as useful models for a variety of physical systems, such as powders [1], porous materials [2], colloidal suspensions [3], liquids [4], and glasses [5].

Numerous experiments have been done to study the packing of spheres. Smith, Foote, and Busang [6] poured lead shots in a glass beaker and used a corrosion technique to mark contacts. For various densities, they counted the number of contacts made by each sphere and reported the frequency of contact numbers. Bernal and co-workers [7,8] used steel ball bearings, which more closely approximate hard spheres, and soaked the packings in paint to mark the contacts. After the paint dried the spheres were broken apart and the number of contacts recorded. In other experiments Bernal and co-workers poured molten wax into the packings and used a modified milling machine to record the coordinates of each sphere in the solidified packings.

Scott and co-workers [9–11] poured ball bearings into cylindrical tubes and carefully measured the packing density as a function of the container size. By extrapolating to infinite size, they arrived at values for the packing density in two reproducible limits. By gently rotating the cylinder into a vertical position, the spheres assembled in a low-density packing termed “loose random packing” (LRP) with a measured packing fraction (volume of the spheres divided by the total volume) of 0.60. By vibrating the cylinders at a suitable frequency for a few minutes, the density had increased to a high-density limit termed “dense random packing” (DRP) with packing fraction of 0.637.

The DRP has been studied extensively. Values of the packing fraction ranging between 0.635 and 0.640 have been reported for a variety of materials, and the radial distribution function and Voronoi analysis of structure have been reported [12]. A derivation of the upper limit of the packing fraction in random hard-sphere packings remains a challenging mathematical problem [1].

Much less is known about the LRP. This is the loosest packing that is stable against compaction under an external load. In the experiments of Scott, Bernal, and others the external load is the gravitational force. Onoda and Liniger [13] recently gave a more fundamental definition of LRP, also taking the limit  $g \rightarrow 0$ , and performed a series of well-defined experiments on glass spheres in liquid mixtures adjusted to include neutrally buoyant conditions. The extrapolated data gave a LRP packing fraction of  $0.555 \pm 0.005$  in the limit of vanishing load.

Spherical colloidal particles with thin polymer coatings interact with a steeply increasing repulsive interaction which closely mimics the hard-sphere system. Light-scattering experiments make it possible to study structure and dynamics in colloidal suspensions in considerable detail. Pusey and van Megen [14] observed “structural arrest” in random packings at a packing fraction of 0.56. This compares reasonably well with molecular-dynamics simulations of hard spheres by Woodcock [15] that indicated a glass transition at a packing fraction of 0.58–0.60. Mode-coupling theories of the hard-sphere system [16,17] predict that a glass transition occurs at a somewhat lower packing fraction, 0.52–0.54.

The structure of the DRP has been applied to model various systems [1]. One of the most successful applications of the DRP structure has been to model metallic and metal-metalloid glasses [18,19]. Cargill [20] showed

that the radial distribution function (RDF) for a one-component DRP agrees remarkably well with the total RDF for amorphous  $\text{Ni}_{76}\text{P}_{24}$  while microcrystalline models do not give good agreement. However, there are some clear differences. The second peak in the total RDF measured for these materials is split into two subpeaks. While the RDF for the hard-sphere packings also has a split second peak, the relative height of the two subpeaks is reversed. In the DRP the second subpeak is higher than the first subpeak, whereas experimental measurements invariably show that the first subpeak is higher.

Many workers have pointed out that relaxation of hard-sphere packings under a model interatomic potential, such as a Lennard-Jones potential, improves the agreement between the DRP model and measurements on metallic glasses. Barker, Hoare, and Finney [21] (BHF) found that relaxation under a Lennard-Jones potential reversed the relative heights of the two subpeaks. It has even been proposed that such relaxation mimics structural changes during annealing of amorphous metals [22].

An important question is how the structure of the LRP compares with that of the DRP. The only detailed study of structural changes accompanying densification that we are aware of is a Voronoi analysis by Finney [23] of a small (500-sphere), computer-simulated cluster. The free surface significantly increases the "configuration space" available to the spheres beyond that available to spheres in a bulk configuration. A very high effective packing fraction was obtained, 0.665, resulting in a reversal of the intensities of the two components of the split second peak.

In this paper we analyze the local structure of the one-component and a two-component random packing of hard spheres using a method that decomposes the RDF according to the local environment of the pairs of spheres. This allows us to identify structural patterns responsible for various features in the RDF and clearly identify spheres in, for example, crystalline and icosahedral environments. In particular, we focus on the structural changes which occur as the density of the packings is gradually increased. Starting with a LRP with a packing fraction of 0.56, we analyze intermediate configurations at increments of 0.02 in the packing fraction, until the densification converges to the DRP limit with a packing fraction of 0.64. We briefly describe the simulations of the hard-sphere packings in Sec. II. In Sec. III we discuss a comparison of the structure of high- and low-density packings with experimental data. While the RDF is itself a rather insensitive and uninformative measure of the structure, it is the starting point for the structural analysis and will be the basis of our discussion. In presenting our results, we begin with the first peak in the RDF and then analyze the second peak. The effect of densification on the radial distribution function is presented in Sec. IV. The decomposition of the RDF using common-neighbor analysis is discussed in Sec. V and its application to one- and two-component hard-sphere packings is presented in Sec. VI. In Sec. VII we compare the one-component hard-sphere packings with Lennard-Jones configurations obtained by relaxation. Section VIII contains a discussion of the results and conclusions.

## II. THE SIMULATIONS

All the hard-sphere configurations consisted of 2000 spheres subject to cubic periodic boundary conditions. The packings were constructed using an algorithm that can briefly be described as follows (a more detailed description is given in Ref. [24]): Random points in a cube are chosen as sphere centers. Radii are assigned so that the initial (nominal) packing fraction is approximately 0.5. In general, the spheres overlap. They are moved sequentially with each move accepted only if it decreases the maximum overlap of the sphere being moved. This is repeated until the maximum overlap among all spheres is nearly zero. Then the radii are increased by a small fraction and this cycle is repeated. Eventually, the spheres become tightly packed and the overlap drops insignificantly over many moves. At this point, the radii are decreased by a very small fraction and the spheres moved to reduce overlaps. The radii are decreased further and the spheres moved until all the overlaps are nearly zero. This cycle of increasing the radii and moving to reduce overlaps, then decreasing radii and moving to reduce overlaps, is repeated many times with decreasing amplitude until the packing fraction at zero overlap converges. Periodically, the spheres are "vibrated" by giving each sphere a small random displacement irrespective of how the overlaps change. That greatly improves the rate of convergence of the calculation.

It is easy to construct a hard-sphere packing with low density on the computer. However, the computer program spends about 90% of the CPU time in going from a packing fraction of 0.60 to 0.64. The structural rearrangements which occur are not trivial, such as simply filling in large holes, but involve rearrangements of groups of spheres to form more compact structures.

Intermediate configurations with packing fractions differing by 0.02 were saved during the densification process for later analysis. By repeating the simulation with different random number seeds, a total of ten one-component runs were made.

While most of the results presented here are for the one-component system, ten packings of a two-component system were simulated and analyzed for comparison. The ratio of diameters of the two component spheres is 1.2 and our 2000 sphere configurations consisted of 80% small spheres. All final configurations of both the one- and two-component systems have a packing fraction of 0.64 in good agreement with the measurements and other computer simulations. Comparison with other simulation algorithms is given in Ref. [24].

## III. COMPARISON WITH EXPERIMENT

A simple measure of the local structure is the number of "contacts" made by the spheres. In Fig. 1(a) a histogram is shown for our computer-simulated packing both for low (0.56) and high (0.64) packing fractions. Not only does the distribution shift to a larger number of contacts as the packing is densified, but the distribution also changes shape. This qualitative change from a nearly symmetric distribution at low packing fraction to a high-

ly asymmetric distribution at higher density was experimentally observed by Smith, Foote, and Busang [6]. However, the agreement is not quantitative, possibly because of the softness of the lead shots used and/or the corrosive technique used in marking the contacts.

A better comparison is with the ball bearings of Bernal and Mason [7]. They reported contact statistics for both the DRP as well as for their LRP with an estimated packing fraction of 0.6. Figure 1(b) shows the comparison of our packing at packing fraction 0.64 with the DRP of Bernal and Mason obtained by shaking and compressing packings of up to 5000 ball bearings. The agreement is quite good. In Fig. 1(c) our simulated packing at 0.60 is compared with their less-dense packing. The agreement is very good, indicating that the simulation produces packings quite similar to both the LRP and the DRP of ball bearings. The cutoff distance used here to define "contact" is 1.057 diameters and was chosen in such a way as to give the same average number of contacts as reported by Bernal and Mason from analyzing the markings on the painted spheres. They estimated their method for determining contacts to be sensitive to pairs separated by 5% of the radius or less, in good

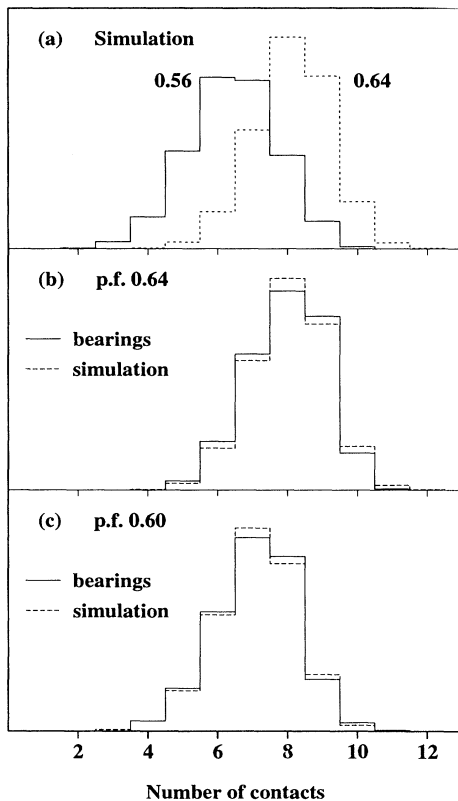


FIG. 1. The figure shows histograms of the number of contacts (meaning  $r < 1.057$ ) made by the spheres in one-component packings. (a) shows the histogram for the computer-simulated packings at a packing fraction (p.f.) of 0.56 (solid line) and 0.64 (dashed line). In (b) and (c) the computer-generated packings (dashed lines) are compared with the packings of steel ball bearings measured by Bernal and Mason (solid lines) [7]. (b) Packing fraction of 0.60, (c) packing fraction of 0.64.

correspondence with our cutoff value.

Finney [12] analyzed the structure of the DRP of ball bearings using the Voronoi method. In the Voronoi cell (or Wigner-Seitz cell) construction [25,26] a polyhedron is defined about each sphere center  $i$ , so that each point of space in the  $i$ th cell is closer to the  $i$ th center than any other center. Two spheres are defined to be neighbors if they share a Voronoi cell face. The local environment of each atom is characterized by the number of faces per cell, the number of edges per face, by the cell volume and surface area. The structure of the dense random packings generated with the algorithm used here is very similar to the structure of the ball-bearing packings analyzed by Finney as measured by Voronoi cell statistics, RDF, and packing fraction (see Ref. [24]). It is also similar by these criteria to other isotropic DRP generated with a somewhat different computer algorithm [27]. Experimental data on hard-sphere LRP's with packing fraction below 0.60 are not available, to our knowledge.

#### IV. THE RADIAL DISTRIBUTION FUNCTION

Figure 2 shows the RDF of the one-component system at an intermediate packing fraction of 0.60 and at the densest packing, 0.64. The difference between the two curves is also shown. All the peaks increase in height and

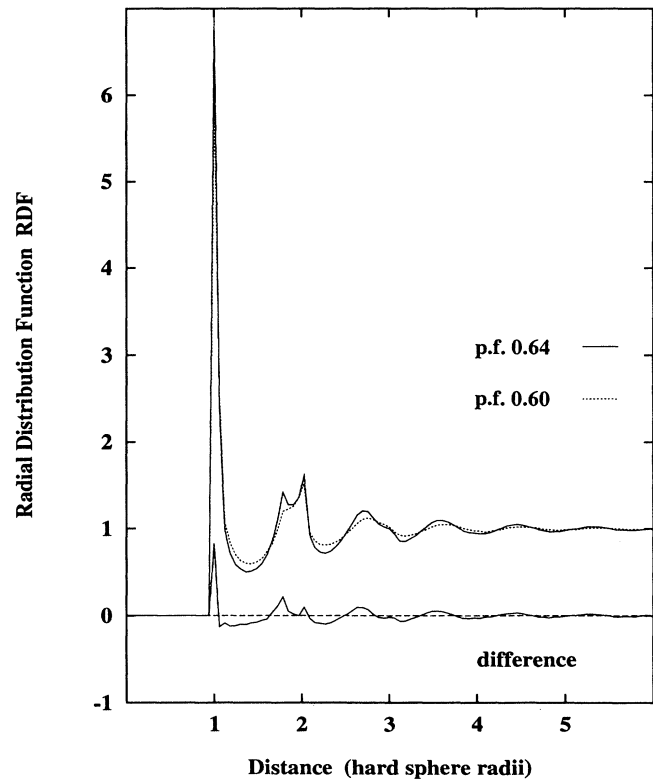


FIG. 2. The RDF at a packing fraction of 0.60 (dotted line) and 0.64 (solid line), averaged over ten one-component configurations. Also shown is the difference between the two (lower solid line). The minima and maxima become more pronounced as the density is increased, but their positions do not change significantly.

the minima deepen, indicating a more-structured packing at the high density, but the positions of maxima and minima remain nearly unchanged.

The clearest change in shape is in the second peak. The splitting of the second peak is characteristic of random packings of spheres. The figure shows that the first subpeak grows more than the second as the packing is densified. This is consistent with the simulation of Finney [23] on a 500-atom cluster, where eventually, at the extremely high packing fractions obtained in the finite cluster, the relative height of the two subpeaks is reversed.

As noted before, the RDF for the simulated packings at a packing fraction of 0.64 agrees very well with the measured RDF for a DRP of ball bearings [12]. Scott, Charlesworth, and Mak [28] reported RDF for a packing of steel balls with a packing fraction of 0.60 as well as for a DRP with a packing fraction of 0.637. While the resolution in those data is too low to separate the two subpeaks, the shape of the second peak changes in a way that is qualitatively consistent with our results: the left side becomes higher, while the right side becomes lower as the packing is densified. Similar changes in the RDF have been observed during thermal annealing of amorphous metals [25,29].

#### V. COMMON-NEIGHBOR ANALYSIS OF STRUCTURE

An essential part of many computer-simulation studies is a powerful technique for systematically analyzing the structure. The method we use, common-neighbor (CN) analysis [30], can be thought of as a decomposition of the RDF according to the environment of the pairs. The first peak of the RDF represents the nearest neighbors. Defining the first peak to be at  $r < r_c$ , where  $r_c$  is the position of the first minimum of the RDF, and referring to those as “bonded” pairs, each pair of atoms is systematically classified in the following way: A set of three indices  $ijkl$  specifies the local environment of the pair. The first index  $j$  is the number of neighbors common to both atoms. The second index  $k$  is the number of bonds between the common neighbors. The third index  $l$  is the number of bonds in the longest continuous chain formed by the  $k$  bonds between common neighbors (see Fig. 5 for examples). After each pair has been assigned to one of the various  $ijkl$  types, the distribution of distances can be calculated in the usual way and a radial distribution function for each type of pairs obtained,  $g_{ijkl}(r)$ . These will be referred to as the CN components of the RDF function and are normalized in such a way that the RDF can then be written as

$$g(r) = \sum_{j,k,l} g_{ijkl}(r).$$

This method can be used to interpret various features in the RDF. In a two-component system, a cutoff  $r_c$  is found for each of the partial distribution functions  $g_{AA}(r)$ ,  $g_{BB}(r)$ , and  $g_{AB}(r)$  and the CN components labeled  $g_{AAijkl}$ ,  $g_{BBijkl}$ , and  $g_{ABijkl}$ .

When the distribution itself is not of interest, the total

number of pairs corresponding to each peak in the RDF is an efficient measure of the structure. Pairs corresponding to the first peak in the RDF are denoted  $\alpha\ jkl$  and their number,  $N_{\alpha\ jkl}$ , is given by

$$N_{\alpha\ jkl} = \frac{4\pi N}{V} \int_0^{r_c} r^2 g_{ijkl}(r) dr.$$

Similarly, pairs corresponding to the second peak, between  $r_c$  and the second minimum in RDF, are denoted by  $\beta\ jkl$ . An earlier and simpler version of this kind of structure analysis was used by Blaisten-Barojas [31] to analyze three-body contributions to the energy of small clusters. Honeycutt and Andersen [32] extended the method and used it to analyze the structure of various stable configurations of one-component LJ clusters. Jónsson and Andersen [33] used the method to identify structural relaxations in one- and two-component LJ liquids.

This method has several advantages over other methods we are aware of. It has a simple interpretation, the number of types of features is manageable and yet it is powerful enough to clearly distinguish between various local structures, in particular fcc, hcp, and icosahedral environments. Different types of pairs are associated with different types of local order. For example, bonded pairs of type 555 are characteristic of icosahedral order, whereas 421 and 422 pairs are characteristic of fcc and hcp order. The only bonded pairs in the fcc crystal are 421, while the hcp crystal has equal numbers of 421 and 422. The difference between the two pairs is the arrangement of the two bonds between the four neighbors. In 421 each of the neighbors forms one of those bonds, in 422 one of the neighbors forms two, two neighbors form one, and the fourth neighbor does not participate in either of the two bonds. While the highly symmetric crystalline packings cause singularities in the Voronoi construction and minor perturbations in the coordinates dramatically change the Voronoi statistics, the common-neighbor analysis is quite insensitive to small displacements of the spheres.

Since the cutoff  $r_c$  is chosen to be the position of a minimum in the RDF, the results of the CN analysis are relatively insensitive to small changes in  $r_c$ . However, in hard-sphere systems there is no preferred distance between spheres since there is no attractive interaction at long range. The first minimum in the RDF is therefore not as deep in hard-sphere packings as in LJ packings, for example. This, in turn, means that the distinction between “bonded” and “nonbonded” pairs is not as clear. However, a similar problem affects other useful measures of short-range order that we are aware of. For instance, in the Voronoi cell construction, an arbitrary cutoff is frequently used [25] to narrow down the definition of a bond. Two spheres that share a Voronoi cell face are only considered to be neighbors if the face has an area bigger than a certain cutoff.

Fortunately, the position of the first minimum in the RDF does not change significantly over the range of packing fractions studied here. Therefore, we consistently use the same cutoff distance for all configurations of the same type. In the one-component hard-sphere system

TABLE I. Cutoff distance  $r_c$  used in the common-neighbor analysis. The hard-sphere cutoffs are relative to the (smaller) hard-sphere diameter  $d_{AA}$ . The Lennard-Jones cutoffs are relative to the (smaller) zero of the potential function  $\sigma_{AA}$ .

	One component	Two component		
		AA	AB	BB
Hard spheres	1.35	1.35	1.46	1.54
Lennard-Jones	1.40	1.40	1.54	1.68

we use  $r_c = 1.35$  diameters. The values of  $r_c$  for the various systems are given in Table I.

## VI. RESULTS OF COMMON-NEIGHBOR ANALYSIS

### A. The first RDF peak

Figure 3(a) shows the relative numbers of various kinds of pairs corresponding to the first peak in the RDF,  $N_{\alpha jkl}$ , as the packing fraction is increased from 0.56 to 0.64 in the one-component system. The coordination number increases from 10.9 to 12.4 over this range. To reduce the effect of the overall increase in the number of bonded pairs, the relative numbers,  $N_{\alpha jkl}/N_{\alpha}$ , are reported. All pairs with more than 5% abundance at packing fraction of 0.64 are shown.

The relative number of 555 and 544 pairs more than doubles as the packing fraction increases from 0.56 to 0.64. A smaller increase occurs in the number of 433 pairs. However, the number of 421 and 422 pairs, which are characteristic of fcc and hcp crystals, remains nearly constant, showing that local crystalline order does not increase. The increased packing efficiency in going from LRP to DRP is therefore entirely different from an approach toward the optimal, crystalline configurations. A dramatic decrease is found in the 311 and 321 pairs. The 321 pairs (not shown) are roughly half as abundant as the 311 at all packing fractions.

All bonded pairs in an icosahedral arrangement of 13 spheres are 555 pairs—the central sphere forms a 555 pair with each of its 12 neighbors. The increased abundance of this pair indicates increased icosahedral order in the sense that fragments of icosahedra involving seven spheres become more numerous. A regular 555 fragment has the structure of a pentagonal bipyramid, with a fivefold-symmetry axis.

The icosahedral arrangement of 12 spheres around a central one is a very efficient one. The outer spheres are not in contact but are separated from each other by a gap amounting to 5% of the sphere diameter [34,35]. This is not the case with 13-sphere clusters carved out of fcc and hcp packings, where the outer spheres are in contact with four other outer spheres. The gap between the outer spheres in the icosahedron can be used to squeeze more spheres in towards the central one. Since there is no preferred distance between hard spheres there is no penalty in rolling the 12 spheres around on the central one in such a way as to enlarge this gap in some places and reduce it in others. For example, if the five neighbors of

a 555 pair are all touching, a 7.35° gap is formed [34,35]. If the environment of the icosahedron is not symmetric, this will most likely be preferred so that an additional sphere can be brought closer in. If one bond is broken between a pair of outer spheres in the icosahedron, two of the 555 pairs get transformed into 544 pairs and two get transformed into 433 pairs. The observed increase in the 544 and 433 pairs is therefore indicative of increased *distorted* icosahedral order.

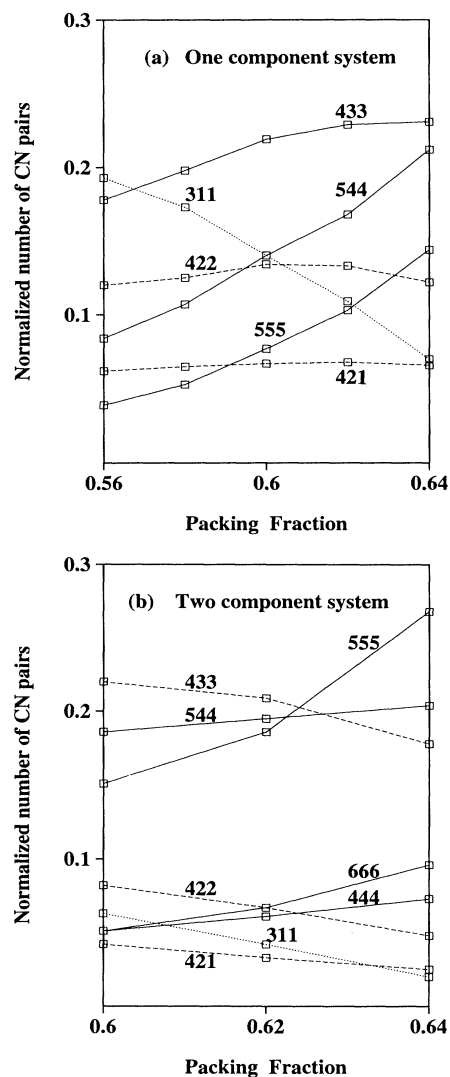


FIG. 3. The relative number (normalized by the total number of bonded pairs) of various CN pairs corresponding to the first peak in the RDF as a function of packing fraction in hard-sphere configurations. (Cutoff distances are given in Table I.) Each data point is an average over ten configurations of 2000 spheres. All pair types amounting to more than 5% of the total in the dense random packing (at 0.64) are shown. (a) One-component system. The number of 555, 544, and 433 pairs increases very significantly with packing fraction. The 322 pairs (not shown) have a similar variation to 311 pairs but are only half as abundant. (b) Binary system with size ratio of 1.2 and 80% small spheres. The number of 555 pairs show the most significant increase.

TABLE II. The number of selected pairs corresponding to the second peak of the RDF in one-component packing of 2000 spheres at various stages of densification. All pairs that give counts larger than 300 at a packing fraction of 0.64 are presented.

Pair type	Packing fraction				
	0.56	0.58	0.60	0.62	0.64
100	19 923	20 061	20 295	20 413	20 461
211	11 511	12 167	12 727	12 902	12 917
322	2198	2387	2405	2177	1788
333	3807	4488	5920	6877	8308
433	452	491	515	510	460
444	559	662	856	1055	1329
455	262	326	528	642	804

The number of complete icosahedra (i.e., 13 sphere clusters, where the central sphere has 12 neighbors and forms a 555 pair with each one) increases with packing fraction but remains fairly small, ca. 10, in the DRP. Typically, some of the icosahedra share a face (with three atoms in common) or interpenetrate (with seven atoms in common) and the total number of atoms in icosahedra is ca. 15% smaller than 13 times the number of icosahedra. No complete icosahedra were found in LRP packings. The number of distorted icosahedra (defined as 13 sphere clusters with the central sphere forming eight 555 pairs, two 544 pairs and two 433 pairs with its neighbors) is approximately twice as high.

Bernal [4] emphasized the importance of tetrahedral order in DRP, but favored structures where the tetrahedra are organized in twisted spirals rather than the spherical clusters related to icosahedral arrangements. These “Bernal spirals,” however, do not include 555 pairs and therefore fail to explain the large increase in the number of those pairs during densification.

Figure 3(b) shows the result for the two-component system. Again, a clear increase in the numbers of bonded 555 pairs is found here, indicating an increase in icosahedral order. The number of 555 pairs is furthermore nearly twice as large as in the one-component system. (Note the narrower range here in the packing fraction—the lower limit is 0.60 rather than 0.56.) However, unlike the one-component case, the numbers of 544 and 433 pairs are nearly constant, and the 666 and, to a lesser extent, the 444 pairs become relatively more abundant. It is not clear how to interpret those results. The latter two pairs are indicative of bcc order. The numbers of other pairs, in particular 421 and 422 pairs, remain nearly constant.

### B. The second RDF peak

An increase in the number of bonded 555 and 544 pairs necessarily affects the abundance of 333 pairs in the second peak of the RDF. Each symmetric  $\alpha$  555 frag-

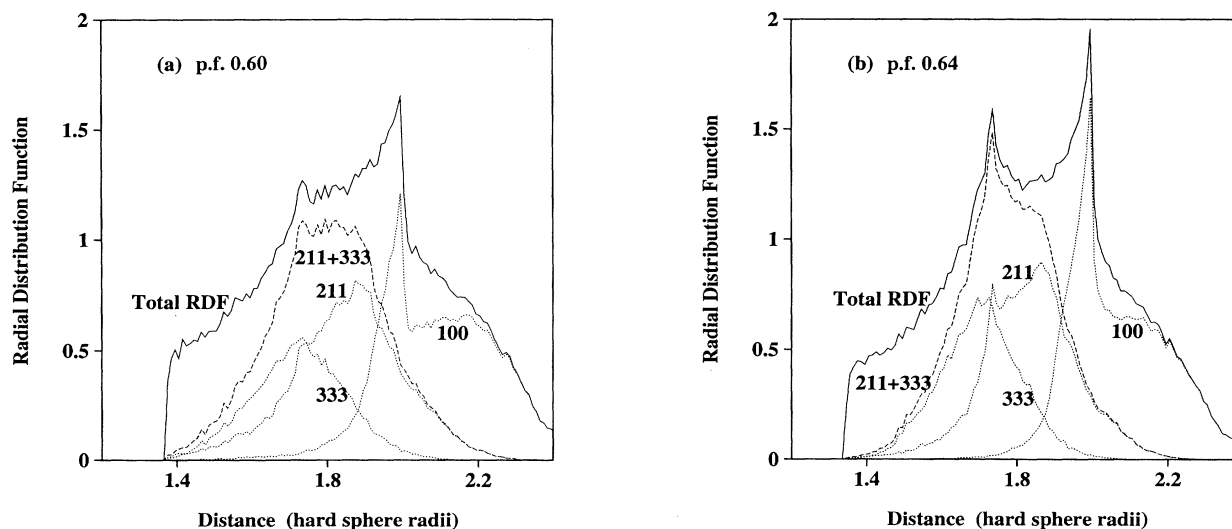


FIG. 4. CN components of the second peak in the RDF for one-component hard-sphere packings (averaged over five configurations). Solid curve, total RDF; dotted curves, the 333, 211, and 100 components; dashed curve, sum of 333 and 211 components. (a) At packing fraction 0.60. The first subpeak is due to 333 pairs (face-sharing tetrahedra) and 211 pairs (adjacent triangles), while the second subpeak is due to 100 pairs (linear trimers). (b) Dense random packing with packing fraction 0.64, otherwise the same as (a). As the density is increased, the 333 pairs increase in abundance and the left shoulder of the 211 peak becomes higher, resulting in a large rise of the first subpeak of the RDF.

ment contains five  $\beta$  333 pairs and a  $\alpha$  544 pair contains two. The  $\alpha$  555 fragment can be regarded as five tetrahedra arranged around a common bonded pair—the  $\beta$  333 pairs are formed by each pair of tetrahedra that share a face.

Table II shows how the total number of the pairs changes with packing fraction. Types that have fewer than 300 pairs in the densest packing are not included. A very large increase is indeed found in the number of 333 pairs, but smaller than is expected from the increased number of 555 and 544 pairs alone. A smaller but significant relative increase is found in 441 and 451 pairs. Other types stay remarkably constant. The 333 pairs in the  $\alpha$  555 fragments can be turned into 444 and 455 pairs by adding another sphere to the side.

The CN components of the RDF directly relate the two subpeaks of the second peak to the local order in the packings. Figure 4 shows the relevant contributions at packing fraction 0.60 (a) and 0.64 (b). The first subpeak (at  $r \approx 1.7$ ) clearly arises roughly equally from 211 pairs (triangles with adjacent sides) and 333 pairs (face-sharing tetrahedra), whereas the second subpeak (at  $r = 2.0$ ) is mainly due to 100 pairs (linear trimers). Figure 5 illustrates the various types of pairs. The abundance of nearly linear trimers of touching spheres is remarkably high. The sharp edge means that trimers with even small gaps between the spheres are rare. Although the relative increase is small, the absolute number of 100 pairs does increase appreciably during densification. The 100 pair is not part of the 555 or 544 fragment, but a complete icosahedron has six 100 pairs (along the six fivefold-rotational axes). Based solely on the position of the two

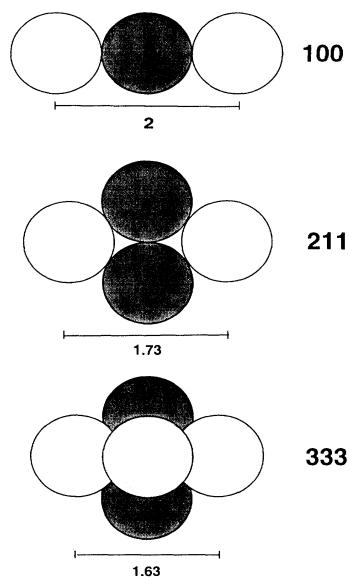


FIG. 5. The three configurations giving the dominant contributions to the second peak in the RDF. The pair is shown with open circles with the distance given below. The shaded circles represent their common neighbors which define the local environment of the pair. The three indices used in the common-neighbor analysis to specify each of the configurations are given to the right.

TABLE III. This table illustrates how 211 and 333 pairs giving rise to the first part of the second peak in the RDF can be interconverted by varying the cutoff distance  $r_c$  in the common-neighbor analysis. The table gives the number of pairs separated by a distance lying in a small interval about the first subpeak [from  $r = 1.70$ – $1.75$ ; see Fig. 4(b)] in a one-component hard-sphere configuration with packing fraction 0.64. The numbers of the four most numerous pairs are given. A substantial fraction of the 211 pairs is converted into 333 pairs as the cutoff is increased.

Cutoff	Pair type			
	100	211	333	454
$r_c = 1.34$	39	1741	1827	75
$r_c = 1.37$	20	1506	2017	150

subpeaks, Finney [12] had proposed the importance of these three geometries, but did not analyze their abundance quantitatively.

The 211 and 333 pairs are quite closely related. A 211 pair can be converted to a 333 pair by bringing in one new neighbor. Therefore, the distinction between 333 and 211 pairs can be quite sensitive to the cutoff distance  $r_c$  used to define neighbors. Table III gives the integrated pair count over a small range in  $r$  about the first subpeak ( $1.70 < r < 1.75$ ) for a slightly smaller (by 1%) and a slightly larger (by 2%) value of the cutoff than otherwise used. There is indeed appreciable conversion of 211 pairs into 333 pairs (ca. 10%) as the cutoff is increased. However, the qualitative picture remains the same.

## VII. COMPARISON OF HARD-SPHERE AND LENNARD-JONES (LJ) RELAXED PACKINGS

A major difference between hard-sphere systems and systems of soft attracting spheres is that no particular distance within the allowed range is preferred between the hard spheres. In order to make a more direct comparison with such systems, we took the coordinates of spheres from the hard-sphere configurations and turned on a Lennard-Jones potential

$$v(r) = 4\epsilon[(\sigma/r)^{12} - (\sigma/r)^6]$$

between the centers. The LJ “atoms” were then allowed to adjust their positions until the force acting on each one vanished. This steepest-descent “relaxation” was done using a molecular-dynamics program, zeroing the kinetic energy of all atoms at each step. It is important to use a small-time step size in order to bring the system into the nearest local minimum on the potential surface. A very small step size was used initially (as small as  $10^{-5}$ ) but it was gradually increased as the relaxation progressed.

This kind of relaxation has frequently been used to bring the structure of hard-sphere packings into closer correspondence with that of amorphous solids [19]. Barker, Hoare, and Finney [21] (BHF) relaxed a one-component 999 hard-sphere cluster under a Lennard-Jones potential and found that the relative heights of the two subpeaks in the split second peak of the RDF reversed during the relaxation. This brought the calculated

RDF into closer agreement with measured RDF's for metal and metal-metalloid glasses [18,19]. The rms displacement of the atoms during relaxation amounted to about 20% of the average nearest-neighbor distance. Voronoi cell analysis showed that this was accompanied by an increase in the number of five-edged faces, suggesting increased icosahedral order [21].

We did relaxation at zero pressure. Choosing  $\epsilon = \sigma = 1$ , we scaled the initial volume in such a way as to bring the pressure to zero. We expected that relaxation of our hard-sphere samples would produce smaller rms displacements than those of BHF because our samples are subject to cubic periodic boundary conditions, allowing the atoms less freedom than at the cluster surface. We also expected that the packing-fraction differences in the hard-sphere configurations would result in density differences in the relaxed Lennard-Jones configurations. In fact, neither of these expectations was realized. We obtained rms displacements approximately twice as large as those of BHF and the relaxation destroyed the structural differences between packings at different densities. The average volume after relaxing ten hard-sphere configurations with a packing fraction of 0.60 was found to be 1965.5 with a standard deviation of 1.0. Repeating this with ten configurations with a packing fraction of 0.64, the average final volume was 1965.0 with a standard deviation of 1.7. The difference between the final densities for the two groups is insignificant although the initial density was significantly different.

Despite these rather drastic changes during relaxation, the numbers of bonded 555 and 544 and 333 pairs remained remarkably constant as the DRP configurations were relaxed. (The relative number of a few CN pair types before and after relaxation is given in Table IV.) Similarly, the number of 333 pairs corresponding to the second RDF peak decreased only slightly, by less than 1%. However, the numbers of bonded 421 and 422 pairs increased dramatically. It is tempting to interpret this in terms of a fairly rigid network of bonded 555 and 544 pairs that form in the DRP and is stable under the relaxation.

The lower-density packings underwent much larger changes in the structure. In fact, the relaxed configurations have nearly the same numbers of CN pairs as the relaxed DRP (see Table IV). The number of complete icosahedra roughly doubles, but the average number of fcc+hcp atoms increased much more dramatically, from 0.5 to 16.5. We conclude that relaxation of the one-component hard-sphere packings mainly enhances local crystalline order.

For comparison, we used two other schemes for the steepest-descent relaxation: (1) constant-volume relaxation and (2) high-pressure relaxation. In all cases the rms displacements during relaxation were very large, of the order of  $0.4\sigma$ . The constant-volume relaxations necessarily preserved density differences, but did not preserve structural differences. The high-pressure relaxations preserved neither density nor structural differences.

In agreement with BHF, we found that relaxation of the DRP at zero pressure reverses the relative heights of the two subpeaks in the split second peak of the RDF.

TABLE IV. Comparison of local structure before and after relaxation under LJ interaction at zero pressure. The number of selected pair types corresponding to the first peak in the RDF is given (normalized by total number of bonded pairs  $N_\alpha$ ). All data are averages over ten one-component configurations with 2000 spheres. The normalized pair counts for the two packing fractions 0.60 and 0.64 differ significantly in the hard-sphere model (HS) before relaxation, but are approximately the same after relaxation. For the dense random packing (0.64), the abundance of pairs characteristic of crystalline order, 421 and 422, increases during relaxation, while the abundance of pairs characteristic of icosahedral order, 555 and 544, is nearly unchanged.

	Pair type			
	422	421	544	555
HS ( $\rho=0.60$ )	0.134	0.067	0.140	0.077
Relaxed HS	0.162	0.094	0.203	0.157
HS ( $\rho=0.64$ )	0.122	0.066	0.212	0.144
Relaxed HS	0.169	0.103	0.201	0.146

However, this is not due to a change in the overall number of the pairs but rather because of a change in the shape of the distribution of distances within the different pair types. The CN components of the RDF after relaxation are shown in Fig. 6 and should be compared with Fig. 4(b). The distribution of distances in 333 pairs and 211 pairs becomes narrower and taller as spheres are pulled and pushed into local potential-energy minima.

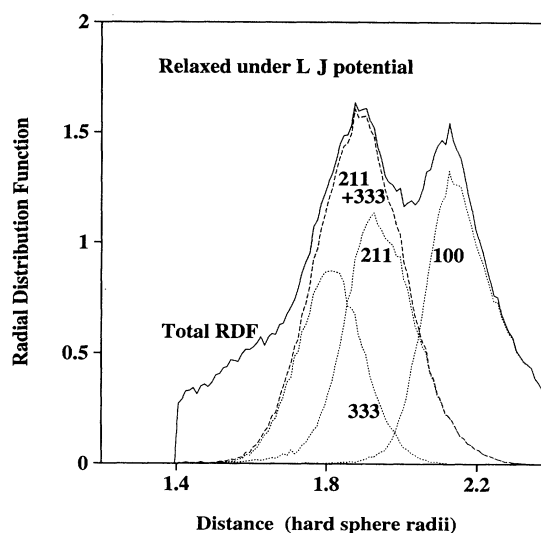


FIG. 6. CN components of the second RDF peak in one-component LJ packings obtained by relaxing dense random packings of hard spheres (packing fraction 0.64) at zero pressure (averaged over five configurations). The various curves have the same meaning as in Fig. 4. While the total number of each type of pair remains nearly constant (decreases by 2% or less), the distribution of distances in 211 and 333 pairs sharpens and the 100 distribution broadens as compared with the original hard-sphere packings [Fig. 4(b)]. The net result is the reversal of the relative height of the first and second subpeaks.

TABLE V. This table illustrates the sensitivity of common-neighbor analysis to the choice of cutoff distance. The logarithmic derivative  $r_c/N_{\alpha jkl}(dN_{\alpha jkl}/dr_c)$  of the number of various bonded pairs with respect to cutoff distance is given for one-component DRP and Lennard-Jones packings. The numbers of 421 and 422 pairs increase with increasing cutoff, whereas the numbers of 544 and 555 pairs decrease. The change is larger in the hard-sphere packing than in the Lennard-Jones packings.

	Pair type			
	421	422	544	555
Hard spheres	-13.5	-13.3	9.05	17.4
Lennard-Jones	-8.08	-7.93	7.10	12.2

At the same time, the sharp edge of the linear trimer peak is smoothed out as the contacts become less well defined because of the softness of the repulsive interaction. This leads to the reversal of the relative peak heights.

The sensitivity of the numbers of various CN pairs to changes in cutoff distance provides another measure of the local order. Table V shows the effect of varying the cutoff distance on the CN pair counts both for the DRP and LJ packings. The numbers of bonded 421 and 422 pairs increase with increasing cutoff, whereas the numbers of bonded 544 and 555 pairs decrease. The numbers change more for the hard sphere than the Lennard-Jones packings, illustrating how the definition of bonded pairs is less clear cut in the hard-sphere system.

### VIII. DISCUSSION AND CONCLUSIONS

It has long been proposed that local icosahedral order may be an essential feature of the structure of simple

glasses [19,34,35]. Clear evidence of the importance of icosahedral order was obtained by Jónsson and Andersen [33], who simulated with molecular dynamics the rapid cooling of one- and two-component Lennard-Jones liquids and found a significant increase in local icosahedral order in the supercooled liquid near the glass transition temperature. The normalized numbers of bonded 555 pairs and second-peak 333 pairs increased upon cooling as well as the number of complete icosahedra. For one-component Lennard-Jones packings, they also found that the degree of local icosahedral order is anticorrelated with the degree of local crystalline order.

The structural changes accompanying densification of hard-sphere packings are qualitatively similar to the structural relaxation observed in the supercooled Lennard-Jones liquids. Quantitative differences are in the number of icosahedral fragments, which is larger in the hard-sphere systems, and the number of complete icosahedra, which is only about 20% of that found in the Lennard-Jones glasses.

In the context of metallic glasses, it is frequently asserted that "the reason for the ubiquity of . . . icosahedra is, of course, that these structures are the lowest-energy configurations for small clusters" [19]. The results presented here on hard-sphere systems demonstrate clearly that icosahedral order can arise from packing constraints alone and can be important in systems where attractive interactions are negligible, for example in colloidal suspensions.

### ACKNOWLEDGMENTS

Acknowledgment is made to the Donors of The Petroleum Research Fund, administered by the American Chemical Society, for partial support of this research, and to NSF (Grant No. CHE-9217774).

\*Present address: Department of Chemistry, University of British Columbia, Vancouver, BC, Canada V6T 1Y6.

†Author to whom correspondence should be addressed.

- [1] D. J. Cumberland and R. J. Crawford, *The Packing of Particles* (Elsevier, Amsterdam, 1987).
- [2] M. Shahinpoor, *Powder Technol.* **25**, 163 (1980).
- [3] P. N. Pusey, in *Liquids, Freezing and Glass Transition*, edited by J. P. Hansen *et al.* (North-Holland, Amsterdam, 1991), Chap. 10; K. Ito, H. Nakamura, H. Yosida, and N. Ise, *J. Am. Chem. Soc.* **110**, 6955 (1988).
- [4] J. D. Bernal, *Proc. R. Soc. London, Ser. A* **280**, 299 (1964).
- [5] G. S. Cargill III, in *Amorphous Materials: Modelling of Structure and Properties*, edited by V. Vitek (TMS-AIME, New York, 1983).
- [6] W. O. Smith, P. D. Foote, and P. F. Busang, *Phys. Rev.* **34**, 1271 (1929).
- [7] J. D. Bernal and G. Mason, *Nature* **188**, 910 (1960).
- [8] J. D. Bernal, G. Mason, and K. R. Knight, *Nature* **194**, 958 (1962).
- [9] G. D. Scott, *Nature* **188**, 908 (1960).
- [10] G. D. Scott, *Nature* **193**, 465 (1962).
- [11] G. D. Scott and D. M. Kilgour, *J. Phys. D* **2**, 863 (1969).
- [12] J. L. Finney, *Proc. R. Soc. London, Ser. A* **319**, 479 (1970).
- [13] G. Y. Onoda and E. G. Liniger, *Phys. Rev. Lett.* **64**, 2727 (1990).
- [14] P. N. Pusey and W. van Meegen, *Phys. Rev. Lett.* **59**, 2083 (1987).
- [15] L. V. Woodcock, *Ann. N.Y. Acad. Sci.* **37**, 274 (1981).
- [16] U. Bengtzelius, W. Götze, and A. Sjolander, *J. Phys. C* **17**, 5915 (1984).
- [17] W. Götze, in *Liquids, Freezing and Glass Transition* (Ref. [3]), Chap. 5.
- [18] R. Zallen, *The Physics of Amorphous Solids* (Wiley, New York, 1983).
- [19] S. R. Elliott, *Physics of Amorphous Materials* (Longman, London, 1984).
- [20] G. S. Cargill III, *J. Appl. Phys.* **41**, 12 (1970).
- [21] L. A. Barker, M. R. Hoare, and J. L. Finney, *Nature* **257**, 120 (1975).
- [22] R. Harris and L. J. Lewis, *Phys. Rev. B* **25**, 4997 (1982).
- [23] J. L. Finney, *Mater. Sci. Eng.* **23**, 199 (1976).
- [24] A. S. Clarke, Ph.D. thesis, University of Wisconsin, Madison, 1986; A. S. Clarke and J. D. Wiley, *Phys. Rev. B* **35**, 7350 (1987).
- [25] D. Srolovitz, K. Maeda, S. Takeuchi, T. Egami, and V. Vitek, *J. Phys. F* **11**, 2209 (1981).
- [26] M. R. Hoare, *J. Non-Cryst. Solids* **31**, 157 (1978).
- [27] W. S. Jodrey and E. M. Tory, *Phys. Rev. A* **32**, 2347

- (1985).
- [28] G. D. Scott, A. M. Charlesworth, and M. K. Mak, *J. Chem. Phys.* **40**, 611 (1964).
- [29] D. Srolovitz, T. Egami, and V. Vitek, *Phys. Rev. B* **24**, 6936 (1981).
- [30] D. Faken and H. Jónsson (unpublished). A computer program for carrying out CN structure analysis with the option of 3D visualization is available upon request from H. Jónsson.
- [31] E. Blaisten-Barojas, *Kinam* **6A**, 71 (1984).
- [32] J. D. Honeycutt and H. C. Andersen, *J. Phys. Chem.* **91**, 4950 (1987).
- [33] H. Jónsson and H. C. Andersen, *Phys. Rev. Lett.* **60**, 2295 (1988).
- [34] D. R. Nelson, *Phys. Rev. B* **28**, 5515 (1983).
- [35] D. R. Nelson and F. Spapen, in *Solid State Physics: Advances in Research and Applications*, edited by H. Ehrenreich and D. Turnbull (Academic, Boston, 1989), Vol. 42, p. 1.

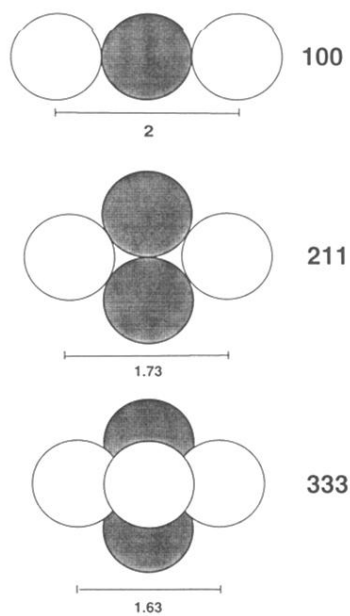


FIG. 5. The three configurations giving the dominant contributions to the second peak in the RDF. The pair is shown with open circles with the distance given below. The shaded circles represent their common neighbors which define the local environment of the pair. The three indices used in the common-neighbor analysis to specify each of the configurations are given to the right.